

DESY-09-191

May 31, 2018

A QCD analysis of ZEUS diffractive data

ZEUS Collaboration

Abstract

ZEUS inclusive diffractive cross-section measurements have been used in a DGLAP next-to-leading-order QCD analysis to extract the diffractive parton distribution functions. Data on diffractive dijet production in deep inelastic scattering have also been included to constrain the gluon density. Predictions based on the extracted parton densities are compared to diffractive charm and dijet photoproduction data.

The ZEUS Collaboration

S. Chekanov, M. Derrick, S. Magill, B. Musgrave, D. Nicholass¹, J. Repond, R. Yoshida
*Argonne National Laboratory, Argonne, Illinois 60439-4815, USA*ⁿ

M.C.K. Mattingly

Andrews University, Berrien Springs, Michigan 49104-0380, USA

P. Antonioli, G. Bari, L. Bellagamba, D. Boscherini, A. Bruni, G. Bruni, F. Cindolo,
M. Corradi, G. Iacobucci, A. Margotti, R. Nania, A. Polini

INFN Bologna, Bologna, Italy^e

S. Antonelli, M. Basile, M. Bindi, L. Cifarelli, A. Contin, S. De Pasquale², G. Sartorelli,
A. Zichichi

University and INFN Bologna, Bologna, Italy^e

D. Bartsch, I. Brock, H. Hartmann, E. Hilger, H.-P. Jakob, M. Jüngst, A.E. Nuncio-Quiroz,
E. Paul, U. Samson, V. Schönberg, R. Shehzadi, M. Wlasenko

Physikalisches Institut der Universität Bonn, Bonn, Germany^b

J.D. Morris³

H.H. Wills Physics Laboratory, University of Bristol, Bristol, United Kingdom^m

M. Kaur, P. Kaur⁴, I. Singh⁴

Panjab University, Department of Physics, Chandigarh, India

M. Capua, S. Fazio, A. Mastroberardino, M. Schioppa, G. Susinno, E. Tassi⁵

Calabria University, Physics Department and INFN, Cosenza, Italy^e

J.Y. Kim⁶

Chonnam National University, Kwangju, South Korea

Z.A. Ibrahim, F. Mohamad Idris, B. Kamaluddin, W.A.T. Wan Abdullah

Jabatan Fizik, Universiti Malaya, 50603 Kuala Lumpur, Malaysia^r

Y. Ning, Z. Ren, F. Sciulli

Nevis Laboratories, Columbia University, Irvington on Hudson, New York 10027, USA^o

J. Chwastowski, A. Eskreys, J. Figiel, A. Galas, K. Olkiewicz, B. Pawlik, P. Stopa,
L. Zawiejski

*The Henryk Niewodniczanski Institute of Nuclear Physics, Polish Academy of Sciences,
Cracow, Poland*ⁱ

L. Adamczyk, T. Bołd, I. Grabowska-Bołd, D. Kisiielewska, J. Łukasik⁷, M. Przybycień,
L. Suszycki

*Faculty of Physics and Applied Computer Science, AGH-University of Science and Technology,
Cracow, Poland*^p

A. Kotański⁸, W. Słomiński⁹

Department of Physics, Jagellonian University, Cracow, Poland

O. Bachynska, O. Behnke, J. Behr, U. Behrens, C. Blohm, K. Borrás, D. Bot, R. Ciesielski, N. Coppola, S. Fang, A. Geiser, P. Göttlicher¹⁰, J. Grebenyuk, I. Gregor, T. Haas, W. Hain, A. Hüttmann, F. Januschek, B. Kahle, I.I. Katkov¹¹, U. Klein¹², U. Kötz, H. Kowalski, V. Libov, M. Lisovyi, E. Lobodzinska, B. Löhner, R. Mankel¹³, I.-A. Melzer-Pellmann, S. Miglioranza¹⁴, A. Montanari, T. Namsoo, D. Notz, A. Parenti, A. Raval, P. Roloff, I. Rubinsky, U. Schneekloth, A. Spiridonov¹⁵, D. Szuba¹⁶, J. Szuba¹⁷, T. Theedt, J. Tomaszewska¹⁸, A. Verbytskyi, G. Wolf, K. Wrona, A.G. Yagües-Molina, C. Youngman, W. Zeuner¹³

Deutsches Elektronen-Synchrotron DESY, Hamburg, Germany

V. Drugakov, W. Lohmann, S. Schlenstedt

Deutsches Elektronen-Synchrotron DESY, Zeuthen, Germany

G. Barbagli, E. Gallo

INFN Florence, Florence, Italy^e

P. G. Pelfer

University and INFN Florence, Florence, Italy^e

A. Bamberger, D. Dobur, F. Karstens, N.N. Vlasov¹⁹

Fakultät für Physik der Universität Freiburg i.Br., Freiburg i.Br., Germany^b

P.J. Bussey, A.T. Doyle, M. Forrest, D.H. Saxon, I.O. Skillicorn

Department of Physics and Astronomy, University of Glasgow, Glasgow, United Kingdom^m

I. Gialas²⁰, K. Papageorgiu

Department of Engineering in Management and Finance, Univ. of the Aegean, Chios, Greece

U. Holm, R. Klanner, E. Lohrmann, H. Perrey, P. Schleper, T. Schörner-Sadenius, J. Sztuk, H. Stadie, M. Turcato

Hamburg University, Institute of Exp. Physics, Hamburg, Germany^b

K.R. Long, A.D. Tapper

Imperial College London, High Energy Nuclear Physics Group, London, United Kingdom^m

T. Matsumoto²¹, K. Nagano, K. Tokushuku²², S. Yamada, Y. Yamazaki²³

Institute of Particle and Nuclear Studies, KEK, Tsukuba, Japan^f

A.N. Barakbaev, E.G. Boos, N.S. Pokrovskiy, B.O. Zhautykov

Institute of Physics and Technology of Ministry of Education and Science of Kazakhstan, Almaty, Kazakhstan

V. Aushev²⁴, M. Borodin, I. Kadenko, Ie. Korol, O. Kuprash, D. Lontkovskiy, I. Makarenko, Yu. Onishchuk, A. Sali, Iu. Sorokin, V. Viazlo, O. Volynets, O. Zenaiev, M. Zolko
Institute for Nuclear Research, National Academy of Sciences, and Kiev National University, Kiev, Ukraine

D. Son
Kyungpook National University, Center for High Energy Physics, Daegu, South Korea^g

J. de Favereau, K. Piotrkowski
Institut de Physique Nucléaire, Université Catholique de Louvain, Louvain-la-Neuve, Belgium^q

F. Barreiro, C. Glasman, M. Jimenez, J. del Peso, E. Ron, J. Terrón, C. Uribe-Estrada
Departamento de Física Teórica, Universidad Autónoma de Madrid, Madrid, Spain^l

F. Corriveau, J. Schwartz, C. Zhou
Department of Physics, McGill University, Montréal, Québec, Canada H3A 2T8^a

T. Tsurugai
Meiji Gakuin University, Faculty of General Education, Yokohama, Japan^f

A. Antonov, B.A. Dolgoshein, D. Gladkov, V. Sosnovtsev, A. Stifutkin, S. Suchkov
Moscow Engineering Physics Institute, Moscow, Russia^j

R.K. Dementiev, P.F. Ermolov[†], L.K. Gladilin, Yu.A. Golubkov, L.A. Khein, I.A. Korzhavina, V.A. Kuzmin, B.B. Levchenko²⁵, O.Yu. Lukina, A.S. Proskuryakov, L.M. Shcheglova, D.S. Zotkin
Moscow State University, Institute of Nuclear Physics, Moscow, Russia^k

I. Abt, A. Caldwell, D. Kollar, B. Reiser, W.B. Schmidke
Max-Planck-Institut für Physik, München, Germany

G. Grigorescu, A. Keramidis, E. Koffeman, P. Kooijman, A. Pellegrino, H. Tiecke, M. Vázquez¹⁴, L. Wiggers
NIKHEF and University of Amsterdam, Amsterdam, Netherlands^h

N. Brümmer, B. Bylsma, L.S. Durkin, A. Lee, T.Y. Ling
Physics Department, Ohio State University, Columbus, Ohio 43210, USAⁿ

A.M. Cooper-Sarkar, R.C.E. Devenish, J. Ferrando, B. Foster, C. Gwenlan²⁶, K. Horton²⁷, K. Oliver, A. Robertson, R. Walczak
Department of Physics, University of Oxford, Oxford United Kingdom^m

A. Bertolin, F. Dal Corso, S. Dusini, A. Longhin, L. Stanco
INFN Padova, Padova, Italy^e

R. Brugnera, R. Carlin, A. Garfagnini, S. Limentani
Dipartimento di Fisica dell'Università and INFN, Padova, Italy^e

B.Y. Oh, J.J. Whitmore²⁸

*Department of Physics, Pennsylvania State University, University Park, Pennsylvania
16802, USA*^o

Y. Iga

Polytechnic University, Sagamihara, Japan^f

G. D'Agostini, G. Marini, A. Nigro

Dipartimento di Fisica, Università 'La Sapienza' and INFN, Rome, Italy^e

J.C. Hart

Rutherford Appleton Laboratory, Chilton, Didcot, Oxon, United Kingdom^m

H. Abramowicz²⁹, R. Ingber, S. Kananov, A. Levy, A. Stern

*Raymond and Beverly Sackler Faculty of Exact Sciences, School of Physics, Tel Aviv
University,
Tel Aviv, Israel*^d

M. Ishitsuka, T. Kanno, M. Kuze, J. Maeda

Department of Physics, Tokyo Institute of Technology, Tokyo, Japan^f

R. Hori, N. Okazaki, S. Shimizu¹⁴

Department of Physics, University of Tokyo, Tokyo, Japan^f

R. Hamatsu, S. Kitamura³⁰, O. Ota³¹, Y.D. Ri³²

Tokyo Metropolitan University, Department of Physics, Tokyo, Japan^f

M. Costa, M.I. Ferrero, V. Monaco, R. Sacchi, V. Sola, A. Solano

Università di Torino and INFN, Torino, Italy^e

M. Arneodo, M. Ruspa

Università del Piemonte Orientale, Novara, and INFN, Torino, Italy^e

S. Fourletov³³, J.F. Martin, T.P. Stewart

Department of Physics, University of Toronto, Toronto, Ontario, Canada M5S 1A7^a

S.K. Boutle²⁰, J.M. Butterworth, T.W. Jones, J.H. Loizides, M. Wing

Physics and Astronomy Department, University College London, London, United Kingdom^m

B. Brzozowska, J. Ciborowski³⁴, G. Grzelak, P. Kulinski, P. Łuzniak³⁵, J. Malka³⁵, R.J. Nowak,
J.M. Pawlak, W. Perlanski³⁵, A.F. Żarnecki

Warsaw University, Institute of Experimental Physics, Warsaw, Poland

M. Adamus, P. Plucinski³⁶, T. Tymieniecka³⁷

Institute for Nuclear Studies, Warsaw, Poland

Y. Eisenberg, D. Hochman, U. Karshon

Department of Particle Physics, Weizmann Institute, Rehovot, Israel^c

E. Brownson, D.D. Reeder, A.A. Savin, W.H. Smith, H. Wolfe

Department of Physics, University of Wisconsin, Madison, Wisconsin 53706, USA ⁿ

S. Bhadra, C.D. Catterall, G. Hartner, U. Noor, J. Whyte

Department of Physics, York University, Ontario, Canada M3J 1P3 ^a

- ¹ also affiliated with University College London, United Kingdom
- ² now at University of Salerno, Italy
- ³ now at Queen Mary University of London, United Kingdom
- ⁴ also working at Max Planck Institute, Munich, Germany
- ⁵ also Senior Alexander von Humboldt Research Fellow at Hamburg University, Institute of Experimental Physics, Hamburg, Germany
- ⁶ supported by Chonnam National University, South Korea, in 2009
- ⁷ now at Institute of Aviation, Warsaw, Poland
- ⁸ supported by the research grant No. 1 P03B 04529 (2005-2008)
- ⁹ This work was supported in part by the Marie Curie Actions Transfer of Knowledge project COCOS (contract MTKD-CT-2004-517186)
- ¹⁰ now at DESY group FEB, Hamburg, Germany
- ¹¹ also at Moscow State University, Russia
- ¹² now at University of Liverpool, United Kingdom
- ¹³ on leave of absence at CERN, Geneva, Switzerland
- ¹⁴ now at CERN, Geneva, Switzerland
- ¹⁵ also at Institute of Theoretical and Experimental Physics, Moscow, Russia
- ¹⁶ also at INP, Cracow, Poland
- ¹⁷ also at FPACS, AGH-UST, Cracow, Poland
- ¹⁸ partially supported by Warsaw University, Poland
- ¹⁹ partially supported by Moscow State University, Russia
- ²⁰ also affiliated with DESY, Germany
- ²¹ now at Japan Synchrotron Radiation Research Institute (JASRI), Hyogo, Japan
- ²² also at University of Tokyo, Japan
- ²³ now at Kobe University, Japan
- ²⁴ supported by DESY, Germany
- ²⁵ partially supported by Russian Foundation for Basic Research grant No. 05-02-39028-NSFC-a
- ²⁶ STFC Advanced Fellow
- ²⁷ nee Korcsak-Gorzo
- ²⁸ This material was based on work supported by the National Science Foundation, while working at the Foundation.
- ²⁹ also at Max Planck Institute, Munich, Germany, Alexander von Humboldt Research Award
- ³⁰ now at Nihon Institute of Medical Science, Japan
- ³¹ now at SunMelx Co. Ltd., Tokyo, Japan
- ³² now at Osaka University, Osaka, Japan
- ³³ now at University of Bonn, Germany
- ³⁴ also at Łódź University, Poland

³⁵ member of Łódź University, Poland

³⁶ now at Lund University, Lund, Sweden

³⁷ also at University of Podlasie, Siedlce, Poland

† deceased

- ^a supported by the Natural Sciences and Engineering Research Council of Canada (NSERC)
- ^b supported by the German Federal Ministry for Education and Research (BMBF), under contract Nos. 05 HZ6PDA, 05 HZ6GUA, 05 HZ6VFA and 05 HZ4KHA
- ^c supported in part by the MINERVA Gesellschaft für Forschung GmbH, the Israel Science Foundation (grant No. 293/02-11.2) and the US-Israel Binational Science Foundation
- ^d supported by the Israel Science Foundation
- ^e supported by the Italian National Institute for Nuclear Physics (INFN)
- ^f supported by the Japanese Ministry of Education, Culture, Sports, Science and Technology (MEXT) and its grants for Scientific Research
- ^g supported by the Korean Ministry of Education and Korea Science and Engineering Foundation
- ^h supported by the Netherlands Foundation for Research on Matter (FOM)
- ⁱ supported by the Polish State Committee for Scientific Research, project No. DESY/256/2006 - 154/DES/2006/03
- ^j partially supported by the German Federal Ministry for Education and Research (BMBF)
- ^k supported by RF Presidential grant N 1456.2008.2 for the leading scientific schools and by the Russian Ministry of Education and Science through its grant for Scientific Research on High Energy Physics
- ^l supported by the Spanish Ministry of Education and Science through funds provided by CICYT
- ^m supported by the Science and Technology Facilities Council, UK
- ⁿ supported by the US Department of Energy
- ^o supported by the US National Science Foundation. Any opinion, findings and conclusions or recommendations expressed in this material are those of the authors and do not necessarily reflect the views of the National Science Foundation.
- ^p supported by the Polish Ministry of Science and Higher Education as a scientific project (2009-2010)
- ^q supported by FNRS and its associated funds (IISN and FRIA) and by an Inter-University Attraction Poles Programme subsidised by the Belgian Federal Science Policy Office
- ^r supported by an FRGS grant from the Malaysian government

1 Introduction

Many aspects of diffractive interactions can be described in the framework of quantum chromodynamics (QCD) as long as a hard scale is present, so that perturbative techniques can be used and the dynamics of the processes can be formulated in terms of quarks and gluons. HERA data have contributed significantly to the understanding of such interactions, since events characterised by the diffractive dissociation of virtual photons, $\gamma^*p \rightarrow Xp$, constitute a large fraction ($\approx 10\%$) of the visible cross section in deep inelastic scattering (DIS). Diffractive reactions in DIS are a tool to investigate low-momentum partons in the proton, notably through the study of diffractive parton distribution functions (DPDFs). The latter are the densities of partons in the proton when the final state of the process contains a fast proton of specified four-momentum. A precise knowledge of the DPDFs is an essential input to predictions of hard diffractive processes at the LHC.

Several recent sets of DPDFs [1–4] have been determined in global fits using the conventional DGLAP formalism [5–7] in next-to-leading-order (NLO) QCD. The diffractive structure function, F_2^D , which dominates the cross section, is directly sensitive to the quark density, whereas the gluon density is only indirectly constrained via scaling violations in the inclusive diffractive DIS cross sections. The inclusion of diffractive dijet data provides an additional constraint on the gluon density, since gluons directly contribute to jet production through the boson-gluon fusion process [8].

For this paper, recently published ZEUS inclusive diffractive data [9] and diffractive DIS dijet data [10] were used to extract the DPDFs. The inclusive data were first fitted alone and then in combination with the dijet data. The results are compared to H1 fits [1,2], as well as to ZEUS diffractive charm data [11] and to ZEUS diffractive dijet photoproduction data [12].

2 Theoretical framework

The cross section for diffractive DIS, $ep \rightarrow eXp$, in the one-photon-exchange approximation, can be expressed in terms of the diffractive reduced cross-section $\sigma_r^{D(3)}$:

$$\frac{d\sigma^{ep \rightarrow eXp}}{d\beta dQ^2 dx_P} = \frac{2\pi\alpha^2}{\beta Q^4} \left[1 + (1-y)^2 \right] \sigma_r^{D(3)}(\beta, Q^2, x_P), \quad (1)$$

which depends on the diffractive structure functions, $F_{2/L}^{D(3)}$, as

$$\sigma_r^{D(3)}(\beta, Q^2, x_P) = F_2^{D(3)}(\beta, Q^2, x_P) - \frac{y^2}{1 + (1-y)^2} F_L^{D(3)}(\beta, Q^2, x_P). \quad (2)$$

The kinematic variables used in Eqs. (1) and (2) are defined as follows:

- $Q^2 = -q^2 = -(k - k')^2$, the negative invariant-mass squared of the exchanged virtual photon, where $q = k - k'$ is the difference of the four-momenta of the incoming and outgoing leptons;
- $x_{\mathcal{P}} = (P - P') \cdot q / P \cdot q$, the fraction of the momentum of the proton carried by the diffractive exchange, where P and P' are the four-momenta of the incoming and outgoing protons, respectively;
- $\beta = Q^2 / 2(P - P') \cdot q$, the Bjorken variable defined for the diffractive exchange;
- the inelasticity $y = (q \cdot P) / (k \cdot P)$.

The four-momentum exchanged at the proton vertex, $|t|$, is integrated over in Eqs. (1) and (2).

The QCD factorisation theorem [13–16] allows the diffractive structure functions, $F_{2/L}^{D(3)}$, to be expressed in terms of convolutions of coefficient functions and DPDFs:

$$F_{2/L}^{D(3)}(\beta, Q^2, x_{\mathcal{P}}) = \sum_i \int_{\beta}^1 \frac{dz}{z} C_{2/L,i} \left(\frac{\beta}{z} \right) f_i^D(z, x_{\mathcal{P}}; Q^2), \quad (3)$$

where the sum runs over partons of type i and z is the longitudinal momentum fraction of the parton entering the hard subprocess with respect to the diffractive exchange. In the lowest-order quark-parton model process, $z = \beta$. The inclusion of higher-order processes leads to $\beta < z$. The coefficient functions $C_{2/L,i}$ are the same as in inclusive DIS. In analogy to the usual parton distribution functions, the DPDFs $f_i^D(z, x_{\mathcal{P}}; Q^2)$ are densities of partons of type i with fractional momentum $zx_{\mathcal{P}}$ in a proton, probed with resolution Q^2 in a process with a fast proton in the final state with fractional momentum $(1 - x_{\mathcal{P}})$. The dependence of the DPDFs on the scale Q^2 is given by the DGLAP evolution equations.

Proton-vertex factorisation [17] was adopted to model the $x_{\mathcal{P}}$ dependence of the DPDFs. Two contributions were assumed, called Pomeron and Reggeon, separately factorisable into a term depending only on $x_{\mathcal{P}}$ and a term depending only on z and Q^2 ,

$$f_i^D(z, x_{\mathcal{P}}; Q^2) = f_{\mathcal{P}}(x_{\mathcal{P}}) f_i(z, Q^2) + f_{\mathcal{R}}(x_{\mathcal{P}}) f_i^{\mathcal{R}}(z, Q^2). \quad (4)$$

The flux-factors $f_{\mathcal{P}}$ and $f_{\mathcal{R}}$ describe the emission of the Pomeron and Reggeon from the proton. Such an assumption was shown [9] to work to a good approximation for the data used in this analysis.

3 Analysis method

The DGLAP evolution equations yield the distributions $f_i(z, Q^2)$ of the quarks and gluons at all values of Q^2 , provided the DPDFs are parameterised as functions of z at some starting scale Q_0^2 . The input parameters were fitted to the data by minimising a χ^2 function [8]. Correlated systematic uncertainties were taken into account by using the method described in an earlier ZEUS publication [18].

The QCD evolution was performed with the programs QCDNUM [19] as well as a newly developed package, QCDC¹. The strong coupling constant was set to $\alpha_s(M_Z) = 0.118$. The contribution from heavy quarks was treated within the general-mass variable-flavour-number scheme of Thorne and Roberts (TR-VFNS) [20], which interpolates between the threshold and the high- Q^2 behaviour for heavy quarks. The values of the heavy-quark masses used were $m_c = 1.35$ GeV and $m_b = 4.3$ GeV [8]. The influence of $F_L^{D(3)}$ was accounted for through its NLO dependence on the parton densities.

The NLO QCD predictions for the diffractive structure functions were obtained by convoluting the DPDFs with the QCD coefficient functions. Predictions for the inclusive diffractive reduced cross sections were obtained using Q as the factorisation and renormalisation scales; for the dijet cross sections, Q was taken as the factorisation scale and the transverse energy of the leading jet, E_T^{jet} , as the renormalisation scale. Predictions for the dijet cross sections at the parton level were performed at NLO with DISENT [21] and NLOJET++ [22]. The two programs agree within 5%. These programs can deal with an arbitrary number of flavours but treat all quarks as massless. Thus they match the TR-VFNS at scales much larger than the quark masses, but may give imprecise results for scales close to the mass thresholds. The predictions were corrected for hadronisation effects [23].

3.1 Parameterisation of the DPDFs

The DPDFs were modelled at the starting scale $Q_0^2 = 1.8$ GeV² in terms of quark singlet, $f_+ = \sum_q (f_q + f_{\bar{q}})$, and gluon, f_g , distributions. The neutrality of the diffractive exchange requires $f_{\bar{q}} = f_q$ for all flavours. The light-quark distributions were assumed to be equal, $f_u = f_d = f_s$. The distributions of the c and b quarks were generated dynamically at the scale Q above the corresponding mass threshold, i.e. no intrinsic charm or bottom were assumed. At the starting scale, chosen to be below the charm threshold, the quark-singlet parameterisation is summed over the light-quark distributions, $f_+ = 6f_q$, where q denotes

¹ Computer code developed by W. Slominski.

any of u, d, s and their antiquarks. The distributions were parameterised at Q_0^2 as

$$\begin{aligned} z f_{d,u,s}(z, Q_0^2) &= A_q z^{B_q} (1-z)^{C_q}, \\ z f_g(z, Q_0^2) &= A_g z^{B_g} (1-z)^{C_g}. \end{aligned} \quad (5)$$

An additional factor, $e^{-\frac{0.001}{1-z}}$, was included to ensure that the distributions vanish for $z \rightarrow 1$ even for negative values of $C_{q,g}$.

The x_P dependence was parameterised using Pomeron and Reggeon fluxes

$$f_{P,R}(x_P, t) = \frac{A_{P,R} e^{B_{P,R} t}}{x_P^{2\alpha_{P,R}(t)-1}}, \quad (6)$$

with linear trajectories $\alpha_{P,R}(t) = \alpha_{P,R}(0) + \alpha'_{P,R} t$, where t is the four-momentum transfer at the proton vertex. The flux factors in Eq. (6) were integrated over t between -1 GeV² and the kinematically allowed maximum value, as for a previous ZEUS publication [9]. The values of the parameters which were fixed in the fits are summarised in Table 1. The value of the normalisation parameter A_P was absorbed in $A_{q,g}$. The Reggeon parton densities, f_i^R in Eq. (4), were taken from a parameterisation derived from fits to pion structure-function data [24].

In total, 9 parameters were left free in the fits: $A_{q,g}$, $B_{q,g}$, $C_{q,g}$, the Pomeron and Reggeon intercepts, $\alpha_P(0)$ and $\alpha_R(0)$, and the normalisation of the Reggeon term, A_R .

3.2 Data

Inclusive diffractive data were fitted alone as well as in combination with a sample of diffractive dijet data. The inclusive diffractive reduced-cross-section data [9] used in the fits were selected using two methods: the requirement of a large rapidity gap between the final-state proton and the rest of the hadronic system (LRG sample) and the detection of the final-state proton in the ZEUS leading proton spectrometer (LPS sample)². These data cover photon-proton centre-of-mass energies in the range $40 < W < 240$ GeV, photon virtualities in the range $2 < Q^2 < 305$ GeV² (LRG) and $2 < Q^2 < 120$ GeV² (LPS) and hadronic-final-state masses in the range $2 < M_X < 25$ GeV (LRG) and $2 < M_X < 40$ GeV (LPS). They span the following x_P ranges: $0.0002 < x_P < 0.02$ (LRG) and $0.002 < x_P < 0.1$ (LPS). Both samples are corrected for background from double-diffractive events $ep \rightarrow eXN$, in which the proton also dissociates into a low-mass state, N . The extracted

² The ZEUS measurements obtained with a third selection method based on the analysis of the distribution of the hadronic-final-state mass (M_X method) [25,26] were not included in the fits as this data sample is highly statistically correlated with the LRG sample.

DPDFs hence correspond to the single-diffractive reaction $ep \rightarrow eXp$. Only inclusive data with $Q^2 > 5 \text{ GeV}^2$ were included in the fits. In order to minimise overlap between the two samples, LPS data with $x_{\mathcal{P}} < 0.02$ were excluded from the fit. Reduced cross sections in bins of Q^2 , $x_{\mathcal{P}}$ and β were used. The total number of fitted data points was 229 from the LRG sample and 36 from the LPS sample.

The diffractive dijet sample in DIS [10] used in the fits covers transverse energies $E_T^{\text{jet}} > 4 \text{ GeV}$ and $x_{\mathcal{P}} < 0.03$. Differential cross sections as a function of $z_{\mathcal{P}}^{\text{obs}}$, an estimator of z , in different Q^2 bins were used. The variable $z_{\mathcal{P}}^{\text{obs}}$ was calculated as $z_{\mathcal{P}}^{\text{obs}} = \frac{Q^2 + M_{jj}^2}{Q^2 + M_X^2}$, where M_{jj} is the invariant mass of the dijet system. This sample provided 28 additional points.

The overlaps between the LRG and dijet samples and between the LPS and dijet samples are small. Therefore, the three data sets were considered statistically independent. The following sources of correlated systematic uncertainties were considered:

- LRG data: energy scale, reweighting of the simulation in $x_{\mathcal{P}}$, variation of the energy threshold on the most forward energy-flow object and proton-dissociation background [9];
- LPS data: energy scale, reweighting of the simulation in $x_{\mathcal{P}}$ and t and proton-dissociation background [9];
- dijet data: energy scale and proton-dissociation background [10].

The energy scale was taken to be common for all the data sets. The normalisation uncertainty due to the proton-dissociation background was taken as fully correlated between the LRG and dijet samples.

4 Results

Fits were performed to the data sets described in Section 3.2. Two different parameterisations of the gluon density at the starting scale were used. This is summarised in Table 2.

Two fits were performed to the LRG+LPS data: ‘Standard’, with A_g , B_g and C_g as free parameters; ‘Constant’, with $B_g = C_g = 0$. The corresponding sets of DPDFs are referred to as “ZEUS DPDF S” and “ZEUS DPDF C”, respectively.

Only data with $Q^2 > Q_{\text{min}}^2 = 5 \text{ GeV}^2$ could be fitted within the combined assumptions of DGLAP evolution and proton-vertex factorisation. The quality of the fit drops rapidly for $Q_{\text{min}}^2 < 5 \text{ GeV}^2$, as shown in Fig. 1, where χ^2/ndf obtained for the fit ZEUS DPDF S, for statistical reasons restricted to the LRG data, is presented as a function of Q_{min}^2 . Although the proton-vertex factorisation assumption worked reasonably well at low Q^2

for the LRG data [9], the combination of this assumption with the DGLAP evolution in Q^2 breaks down below Q^2 of 5 GeV^2 . In contrast, in fully inclusive DIS, DGLAP fits were performed successfully [18] down to Q^2 of 2.5 GeV^2 .

The results of the fits are listed in Table 3. In the minimisation procedure, the χ^2 was calculated using only the statistical and uncorrelated systematic errors. The correlated systematic uncertainties were treated according to the “offset method” [18] and were included in the determination of the full experimental uncertainty. To evaluate the goodness of the fit, the χ^2 shown in Table 3 was recalculated by adding the statistical, uncorrelated and correlated systematic errors in quadrature. The number of degrees of freedom in this case corresponds to the number of fitted points.

The inclusive data are sensitive to all three quark-related parameters, A_q , B_q and C_q . However, they show very little sensitivity to the gluon shape (B_g and C_g). This follows from $F_2^{D(3)}$ being directly sensitive only to quarks. The values obtained for $\alpha_{\mathcal{P}}(0)$, $\alpha_R(0)$ and A_R in all fits are fully consistent with those extracted from a fit [9] to the same data based on the proton-vertex factorisation assumption of Eq. (4).

Fits ZEUS DPDF C and S are of equally good quality and the predicted reduced cross sections are indistinguishable. Figures 2–4 show fit S compared to the LRG and LPS data. Both data samples are well described. For $Q^2 < 5 \text{ GeV}^2$, the predictions are extrapolated and underestimate the LRG as well as the LPS data for $x_{\mathcal{P}} < 0.005$. The fit is above the LPS data in the low- β region, where there are no LRG data.

The quark and gluon densities, $zf_q(z, Q^2)$ and $zf_g(z, Q^2)$, from fit S are shown with their experimental uncertainties in the upper (lower) part of Fig. 5 for $Q^2 = 6, 20, 60$ and 200 GeV^2 . The DPDFs from fit C are also shown. The relative normalisation of the Pomeron flux, $f_{\mathcal{P}}$, and of the DPDFs, $f_i(z, Q^2)$, in Eq. (4) is arbitrary; for Fig. 5 the normalisation was chosen such that at $x_{\mathcal{P}} = 0.003$ the quantity $x_{\mathcal{P}} f_{\mathcal{P}}(x_{\mathcal{P}}) = 1$.

The quark distributions are very similar for the two fits while the gluon densities are significantly different. Gluons from fit S grow rapidly at high z , while those from fit C vanish as $z \rightarrow 1$ in a smoother way. The large discrepancy demonstrates the low sensitivity of the inclusive data to gluons. To constrain the gluons better, a more exclusive process is needed where photon-gluon fusion contributes at leading order.

Predictions based on ZEUS DPDF S and C are compared to the double-differential diffractive dijet cross section [10] in Fig. 6. The uncertainty due to the variation of the renormalisation scale in the calculation between $0.5E_T^{\text{jett}}$ and $2E_T^{\text{jett}}$ is also shown. At high $z_{\mathcal{P}}^{\text{obs}}$ the predictions based on fit C give a good description of the dijet data throughout the whole kinematic region. This is not the case for fit S. Figure 6 clearly shows that the dijet data are sensitive to the gluon density.

A third fit was performed to the LRG+LPS data in combination with the dijet data. The

corresponding DPDFs are referred to as “ZEUS DPDF SJ” and the resulting parameters are also given in Table 3. This fit is indistinguishable from fit S when compared to the inclusive data and also provides a remarkably good description of the dijet data, as shown in Fig. 7.

The quark and gluon densities from fit SJ are shown with their experimental uncertainties in Fig. 8 for $Q^2 = 6, 20, 60$ and 200 GeV^2 . The result of fit C is also shown for comparison. Again, the plotted quantities are $z f_{q,g}(z, Q^2)$ with the normalisation $x_{\mathcal{P}} f_{\mathcal{P}}(x_{\mathcal{P}}) = 1$ at $x_{\mathcal{P}} = 0.003$. The decrease in the uncertainty on the gluon distribution with respect to the fit without jet data (Fig. 5) is clearly seen. Combining the inclusive and dijet data constrains the gluon and the quark densities with a comparable precision across the whole z range.

Figure 9 shows the Q^2 dependence of the fraction of the longitudinal momentum of the diffractive exchange carried by the gluons, g_{frac} , according to fit ZEUS DPDF SJ, integrated over the range $10^{-5} < z < 1$. Over the wide range $5 < Q^2 < 300 \text{ GeV}^2$, the fraction amounts to approximately 60%. The fall with Q^2 is a direct consequence of the DGLAP evolution which forces g_{frac} to approach ≈ 0.5 at high Q^2 , while the slope change at $Q = m_b$ reflects the change in the number of flavours from four to five.

4.1 DPDF uncertainties

The following sources of uncertainties were investigated:

- the starting scale Q_0^2 . The value 1.8 GeV^2 was chosen as it minimises the χ^2 . Varying Q_0^2 for fit C between 1.6 and 2 GeV^2 yielded a χ^2 between 1.18 and 1.20 ; the DPDFs did not change significantly;
- the fixed parameters in the fits (Table 1). Variations within the measurement errors resulted in a simple scaling of the fluxes integrated over t , absorbed into the normalisation parameters A_q , A_g and A_R , with negligible effect on the DPDFs;
- the renormalisation scale dependence. The scale μ_R for dijet data was taken as $0.5 E_T^{\text{jct}}$ and $2 E_T^{\text{jct}}$, whereas it was kept as Q for the inclusive data. The effect on the parton densities was within 5% for light quarks, 15% for c and b and 30% for gluons, while the χ^2 increased significantly;
- the masses of the charm and beauty quarks. The nominal values of $m_c = 1.35 \text{ GeV}$ and $m_b = 4.3 \text{ GeV}$ were varied in the ranges $1.35 < m_c < 1.75 \text{ GeV}$ and $4.3 < m_b < 5 \text{ GeV}$. Neither the quark nor gluon distributions were sensitive to variations of m_b , whereas m_c produced an effect comparable to the experimental uncertainty. The χ^2 value changed only slightly, reaching the minimum at the nominal mass values.

These theoretical uncertainties are not shown in Figs. 5, 8 and 9. Given are the total experimental uncertainties as determined with the offset method [18].

4.2 Comparison to other HERA DPDFs

An earlier ZEUS DPDF fit to inclusive diffractive measurements combined with data on charm production [27] did not include data points with values of $\beta > 0.4$. Also, in the current analysis a far larger data sample is used. This previous analysis is therefore superseded by the results of the present paper.

Several DPDF fits are available from the H1 Collaboration, among which the most recent are based on an inclusive diffractive sample [1] and on a combination of data from inclusive and diffractive dijets in DIS [2]. In Fig. 10, the diffractive reduced cross sections from the ZEUS LRG sample as a function of Q^2 for fixed β and x_P are compared to the fit ZEUS DPDF SJ as well as to the predictions from ‘‘H1 2006 Fit B’’ [1]. The latter, extracted for masses of the dissociative system $M_N < 1.6$ GeV, were multiplied by the scaling factor 0.81 [1] to account for the correction to the ZEUS elastic case $M_N = m_p$. For $Q^2 < 5$ GeV² in the ZEUS case and for $Q^2 < 8.5$ GeV² in the H1 case, the fits are extrapolated. For $\beta < 0.2$, the two fits agree in shape throughout the fitted range, but the normalisation of the ZEUS curve is above that of H1. At higher β and where the predictions are extrapolated the agreement worsens. These features reflect the degree of consistency between the ZEUS and H1 data [28].

4.3 Comparison to charm and dijet photoproduction data

Predictions from the fit ZEUS DPDF SJ are compared in Fig. 11 to data [11] on the charm contribution to the diffractive structure function multiplied by x_P , $x_P F_2^{D(3)c\bar{c}}$, for x_P of 0.004 and 0.02 and Q^2 of 4 and 25 GeV². The predictions are in fair agreement with the data.

Figures 12a and 13a show the prediction from the fit ZEUS DPDF SJ compared to the diffractive dijet photoproduction data [12] as a function of x_γ^{obs} , the fraction of the photon energy invested in producing the dijet system, and of the transverse energy E_T^{jet} of the leading jet, respectively. Dijet photoproduction at leading order in QCD proceeds through two type of processes: direct processes ($x_\gamma^{\text{obs}} \approx 1$), in which the exchanged photon interacts as a point-like particle with the partons from the diffractive exchange; and resolved processes ($x_\gamma^{\text{obs}} < 1$), in which the photon behaves as a source of partons which interact with the diffractive exchange. For the latter, as in hadron-hadron interactions, QCD factorisation is not expected to hold [13]. Comparing calculations based on DPDFs

extracted from other diffractive processes to diffractive dijet photoproduction data provides a valuable test of QCD factorisation. The predictions shown in Figs. 12a and 13a, obtained with the program of Klasen and Kramer [29], agree adequately with the data over the whole x_γ^{obs} and E_T^{jct} ranges³. A further confirmation is provided by Figs. 12b and 13b, where the ratio of the data and the predictions is presented as a function of x_γ^{obs} and E_T^{jct} , respectively. The ratio is consistent with unity. This reinforces the conclusion of an earlier ZEUS publication [12], where the data were found to be compatible with no suppression either of the resolved component, or of both components globally. The slight normalisation difference between the predictions shown here and those of the earlier ZEUS publication [12] is due to the usage of different DPDFs (“H1 2006 Fit B”), extracted in a fixed-flavour-number scheme.

Also shown in Figs. 12 and 13 are the predictions from “H1 Fit 2007 Jets” [2], multiplied by the scaling factor 0.81 [1] to account for the correction to $M_N = m_p$. They overlap with the ZEUS predictions in the lowest E_T^{jct} and highest x_γ^{obs} bins. At high E_T^{jct} and low x_γ^{obs} , the two predictions differ by as much as 20%.

5 Summary and conclusions

ZEUS diffractive inclusive cross-section data, together with data on diffractive dijet production in DIS, have been used in a NLO DGLAP QCD analysis to determine the diffractive parton distribution functions. Only data with $Q^2 > 5 \text{ GeV}^2$ could be fitted within the combined framework of DGLAP evolution and proton-vertex factorisation. The extracted DPDFs correspond to the single-diffractive reaction with a proton in the final state and are valid in the region $|t| < 1 \text{ GeV}^2$, $M_X > 2 \text{ GeV}$, $x_{\mathbb{P}} < 0.1$.

NLO QCD predictions based on diffractive parton densities extracted from the inclusive data provide a good, simultaneous description of the inclusive and dijet data. The quark densities are well constrained by the inclusive data, whereas the sensitivity to the gluon density decreases as the momentum fraction z increases.

The inclusion of the dijet data provides an additional constraint on the gluons, allowing the determination of both the quark and gluon densities with good accuracy.

Predictions based on the extracted parton densities give a fair description of diffractive charm production data; also, they are in good agreement with diffractive dijet photoproduction cross sections over the whole kinematic region, thus indicating no suppression of the resolved component.

³ The program of Frixione and Ridolfi [30] was also used and gave the same results.

Acknowledgements

The design, construction and installation of the ZEUS detector were made possible by the ingenuity and dedicated efforts of many people inside DESY and from the home institutes who are not listed as authors. Their contributions are acknowledged with great appreciation. We thank the DESY directorate for their strong support and encouragement, and the HERA machine group for their diligent effort. We are grateful for the support of the DESY computing and network services.

References

- [1] H1 Coll., A. Aktas et al., Eur. Phys. J. **C 48**, 715 (2006).
- [2] H1 Coll., A. Aktas *et al.*, JHEP **0710:042** (2007).
- [3] A.D. Martin, M.G. Ryskin and G. Watt, Phys. Lett. **B 644**, 131 (2007).
- [4] K. Golec-Biernat and A. Luszczak, arXiv:0812.3090 (2008).
- [5] V.N. Gribov and L.N. Lipatov, Sov. J. Nucl. Phys. **15**, 438 (1972).
- [6] Yu.L. Dokshitzer, Sov. Phys. JETP **46**, 641 (1977).
- [7] G. Altarelli and G. Parisi, Nucl. Phys. **B 126**, 298 (1977).
- [8] ZEUS Coll., S. Chekanov *et al.*, Eur. Phys. J. **C42**, 1 (2005).
- [9] ZEUS Coll., S. Chekanov *et al.*, Nucl. Phys. **B 816**, 1 (2009).
- [10] ZEUS Coll., S. Chekanov *et al.*, Eur. Phys. J. **C 52**, 813 (2007).
- [11] ZEUS Coll., S. Chekanov *et al.*, Nucl. Phys. **B 672**, 3 (2003).
- [12] ZEUS Coll., S. Chekanov *et al.*, Eur. Phys. J. **C 55**, 177 (2008).
- [13] J.C. Collins, Phys. Rev. **D 57**, 3051 (1998).
- [14] Erratum, *ibid.* **D 61**, 019902 (2000).
- [15] L. Trentadue and G. Veneziano, Phys. Lett. **B 323**, 201 (1994).
- [16] A. Berera and D.E. Soper, Phys. Rev. **D 53**, 6162 (1996).
- [17] P.D.B. Collins, *An Introduction to Regge Theory and High Energy Physics*. Cambridge University Press, Cambridge (1997).
- [18] ZEUS Coll., S. Chekanov *et al.*, Phys. Rev. **D 67**, 012007 (2003).
- [19] ZEUS Coll., J. Breitweg *et al.*, Phys. Lett. **B 407**, 432 (1997).
- [20] R.S. Thorne and R.G. Roberts, Phys. Rev. **D 57**, 6871 (1998).
- [21] S. Catani and M.H. Seymour, Nucl. Phys. **B 510**, 503 (1998).
- [22] Z. Nagy and Z. Trocsanyi, Phys. Rev. Lett. **87** (2001) 082001.
- [23] A. Bonato, Ph. D. Thesis, Hamburg University, DESY-THESIS-2008-008.
- [24] M. Glück, E. Reya and A. Vogt, Z. Phys. **C 53**, 127 (1992).
- [25] ZEUS Coll., S. Chekanov *et al.*, Nucl. Phys. **B 713**, 3 (2005).
- [26] ZEUS Coll., S. Chekanov *et al.*, Nucl. Phys. **B 800**, 1 (2008).
- [27] ZEUS Coll., S. Chekanov *et al.*, Eur. Phys. J. **C38**, 43 (2004).

- [28] P. Newman and M. Ruspa, *Proc. of the Workshop HERA and the LHC - 2nd Workshop on the implications of HERA for the LHC physics*. H. Jung and A. De Roeck eds., Hamburg (2009), DESY-PROC-2009-002.
- [29] M. Klasen and G. Kramer, *Z. Phys.* **C76**, 67 (1997).
- [30] S. Frixione and G. Ridolfi, *Nucl. Phys.* **B 507**, 315 (1997).
- [31] A. Donnachie and P.L. Landshoff, *Phys. Lett.* **B 296**, 227 (1992).

Parameter	Fixed to	Measurement	Ref.
$\alpha'_{\mathcal{P}}$	0	$-0.01 \pm 0.06(\text{stat.})_{-0.08}^{+0.04}(\text{syst.}) \pm 0.04(\text{model}) \text{ GeV}^{-2}$	[9]
$\alpha'_{\mathcal{R}}$	0.9 GeV^{-2}	$0.90 \pm 0.10 \text{ GeV}^{-2}$	[31]
$B_{\mathcal{P}}$	7.0 GeV^{-2}	$7.1 \pm 0.7(\text{stat.})_{-0.7}^{+1.4}(\text{syst.}) \text{ GeV}^{-2}$	[9]
$B_{\mathcal{R}}$	2.0 GeV^{-2}	$2.0 \pm 2.0 \text{ GeV}^{-2}$	[31]

Table 1: *The values of the parameters fixed in the fits and the measurements providing this input.*

Fit name	Data set	$zg(z)$
ZEUS DPDF S	LRG + LPS	$A_g z^{B_g} (1-z)^{C_g}$
ZEUS DPDF C	LRG + LPS	A_g
ZEUS DPDF SJ	LRG + LPS + DIS dijets	$A_g z^{B_g} (1-z)^{C_g}$

Table 2: *Data sets used and parameterisation of the gluon density at the starting scale for the different fits.*

Parameter	Fit value		Fit value	
	DPDF S		DPDF C	
A_q	0.135	± 0.025	0.161	± 0.030
B_q	1.34	± 0.05	1.25	± 0.03
C_q	0.340	± 0.043	0.358	± 0.043
A_g	0.131	± 0.035	0.434	± 0.074
B_g	-0.422	± 0.066	0	
C_g	-0.725	± 0.082	0	
$\alpha_{\mathcal{P}}(0)$	1.12	± 0.02	1.11	± 0.02
$\alpha_{\mathcal{R}}(0)$	0.732	± 0.031	0.668	± 0.040
$A_{\mathcal{R}}$	2.50	± 0.52	3.41	± 1.27
χ^2/ndf	315/265	= 1.19	312/265	= 1.18
			336/293	= 1.15

Table 3: *Parameters obtained with the different fits and their experimental uncertainties.*

ZEUS

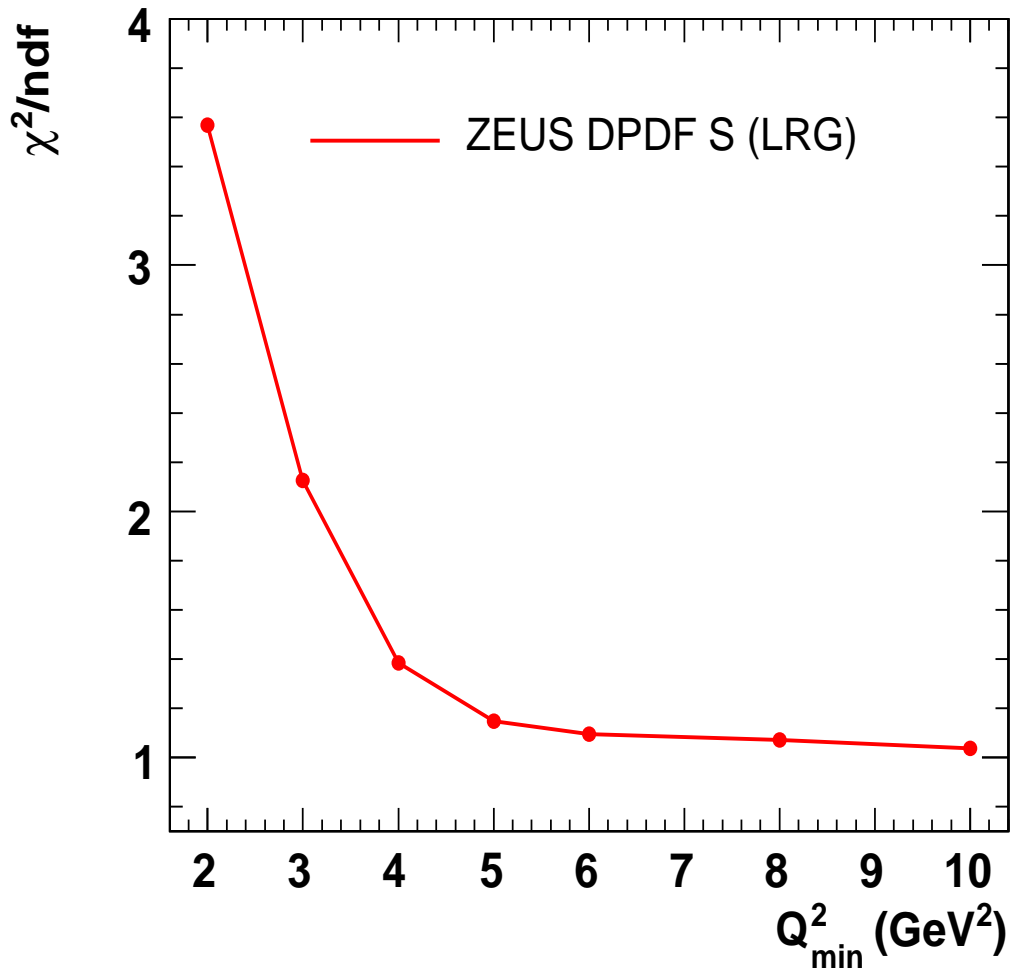


Figure 1: *Dependence of χ^2/ndf for the fit ZEUS DPDF S on the value of the minimum Q^2 , Q^2_{\min} , of the LRG data entering the fit.*

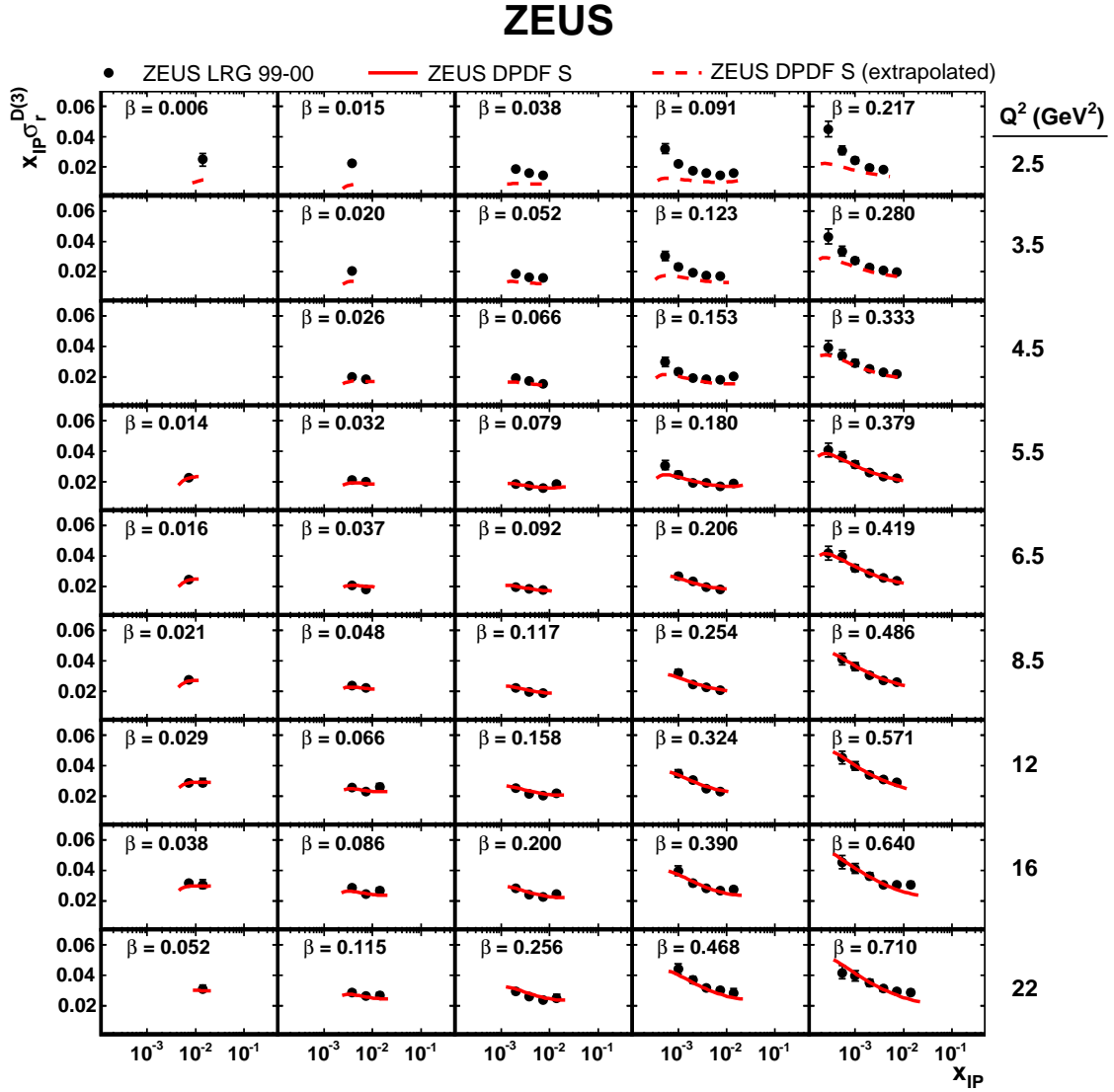


Figure 2: The fit ZEUS DPDF S compared to the ZEUS LRG data [9] as a function of x_{IP} for different β and Q^2 values at low Q^2 . Where visible, the inner error bars show the statistical uncertainties and the full bars indicate the statistical and systematic uncertainties added in quadrature. The dashed lines represent the DGLAP extrapolation beyond the fitted region.

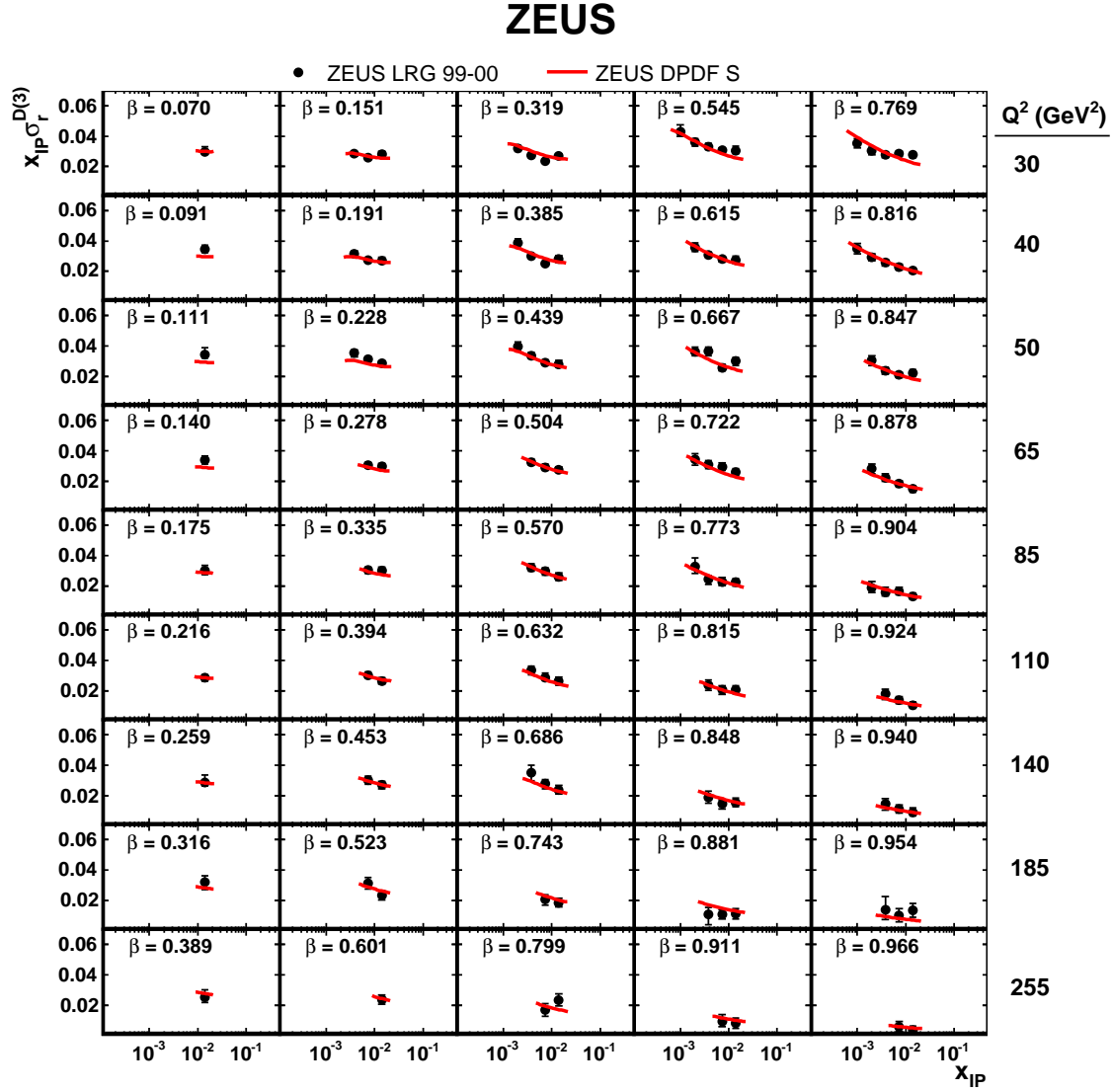


Figure 3: The fit ZEUS DPDF S compared to the ZEUS LRG data [9] as a function of x_P for different β and Q^2 values at high Q^2 . Where visible, the inner error bars show the statistical uncertainties and the full bars indicate the statistical and systematic uncertainties added in quadrature.

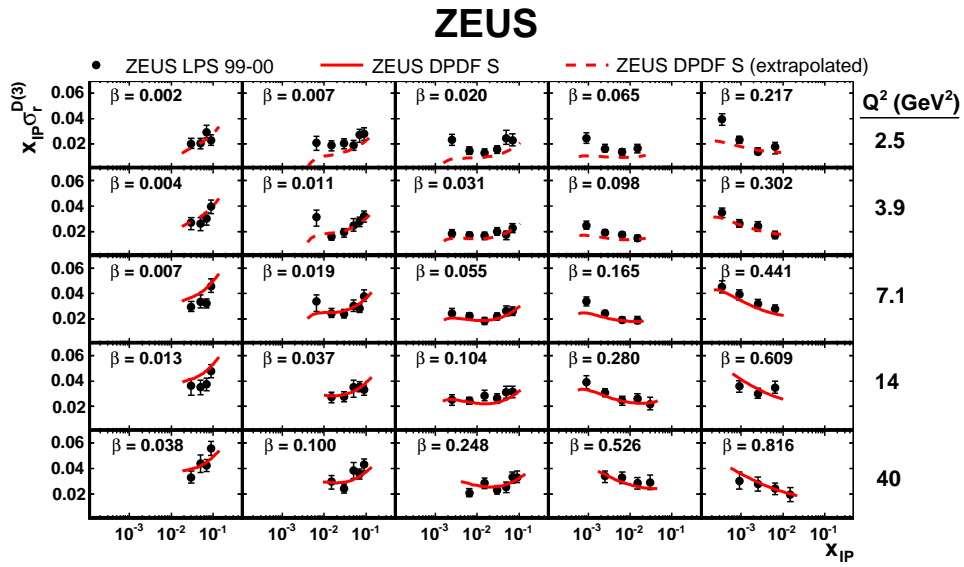


Figure 4: The fit ZEUS DPDF S compared to the ZEUS LPS data [9] as a function of x_P for different β and Q^2 values. The inner error bars show the statistical uncertainties and the full bars indicate the statistical and systematic uncertainties added in quadrature. The dashed lines represent the DGLAP extrapolation beyond the fitted region.

ZEUS

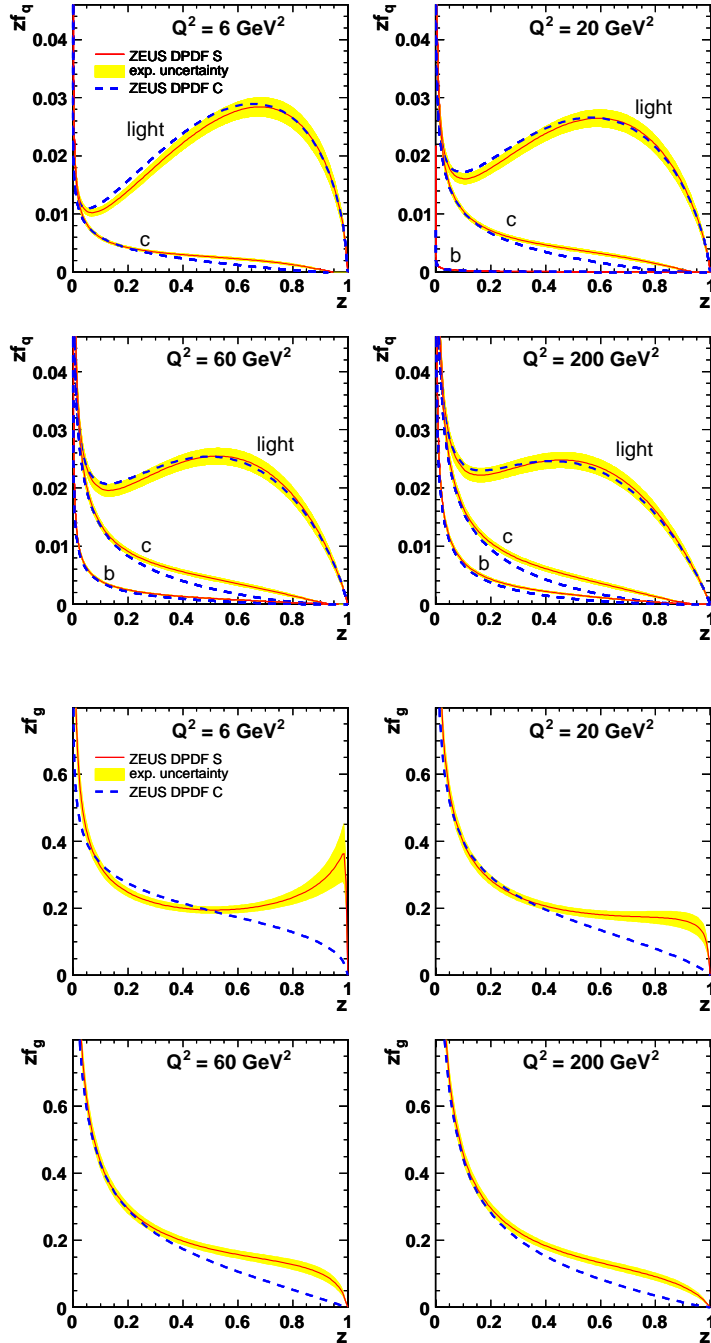


Figure 5: Four upper (lower) plots: the quark (gluon) distributions obtained from fits ZEUS DPDF S (continuous line) and ZEUS DPDF C (dashed line), shown for four different values of Q^2 . The shaded error bands show the experimental uncertainty.

ZEUS

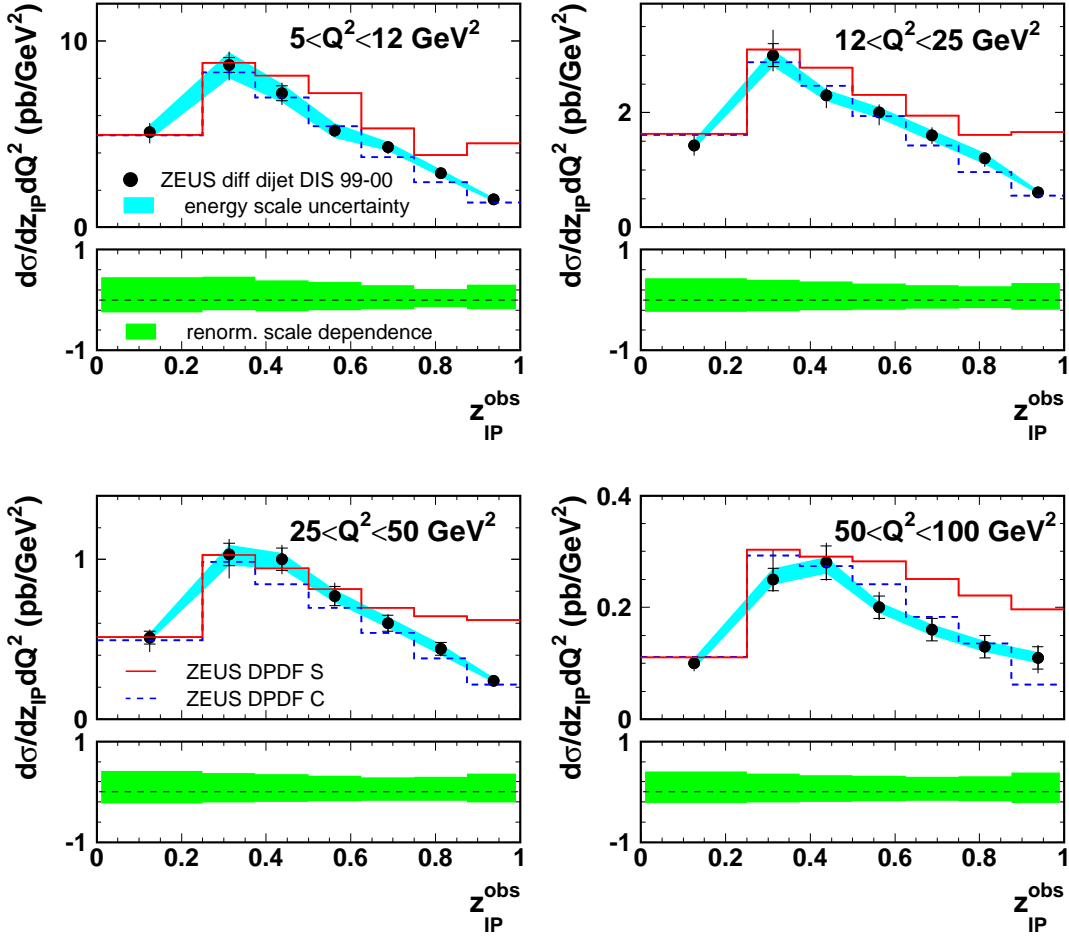


Figure 6: Predictions based on ZEUS DPDF S (continuous line) and ZEUS DPDF C (dashed line) compared to the ZEUS diffractive dijet data [10] as a function of z_{IP}^{obs} for different Q^2 values. The inner error bars show the statistical uncertainties and the full bars indicate the statistical and systematic uncertainties added in quadrature. The dark shaded bands indicate the jet energy scale uncertainty. The light shaded bands at the bottom of each plot show the renormalisation scale uncertainty.

ZEUS

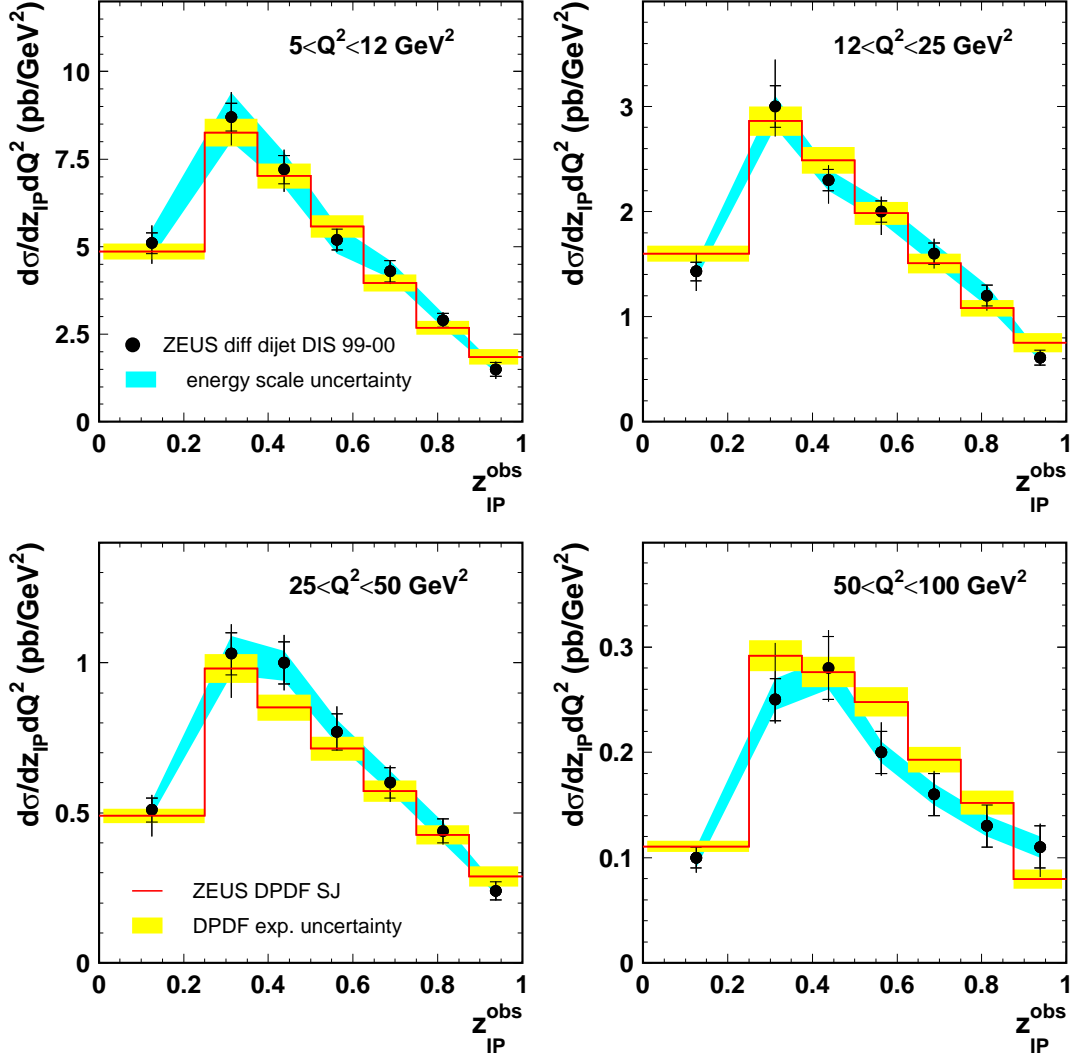


Figure 7: The fit ZEUS DPDF SJ compared to the ZEUS diffractive dijet data [10] as a function of z_{IP}^{obs} for different Q^2 values. The inner error bars show the statistical uncertainties and the full bars indicate the statistical and systematic uncertainties added in quadrature. The dark shaded bands indicate the jet energy scale uncertainty. The light shaded bands show the DPDF experimental uncertainties.

ZEUS

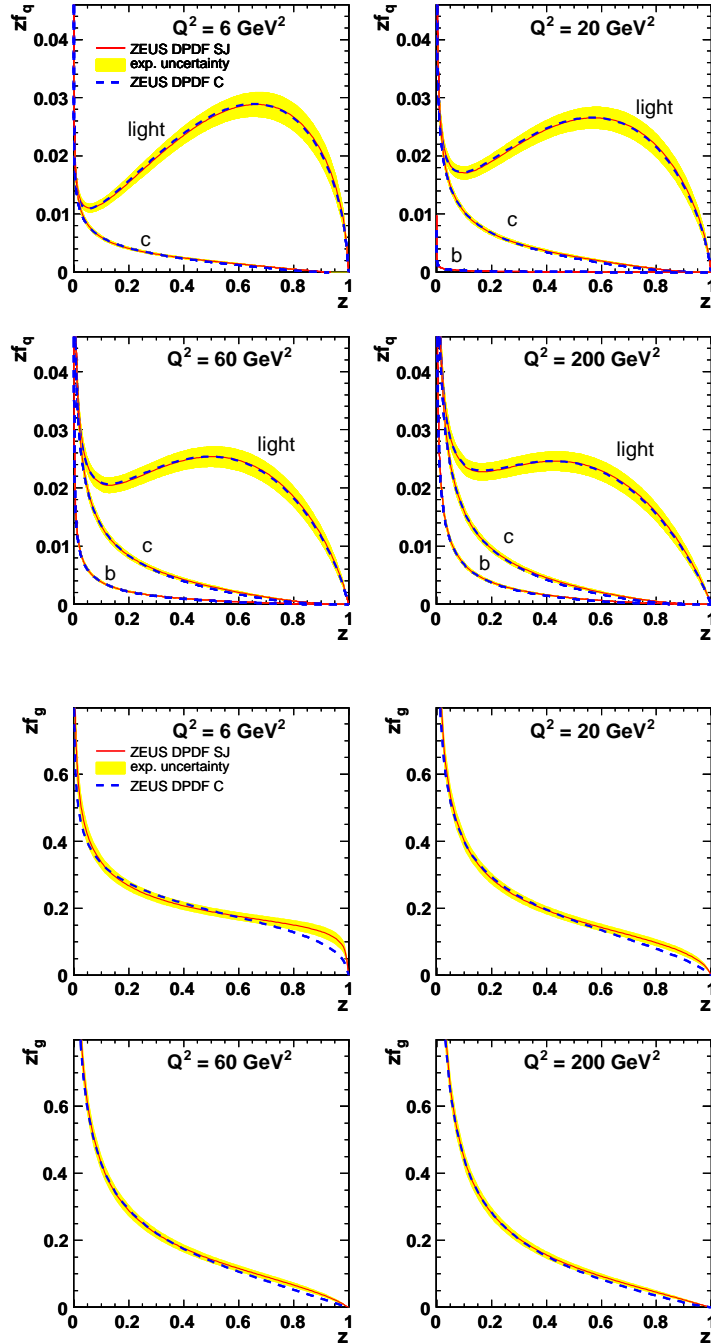


Figure 8: Four upper (lower) plots: the quark (gluon) distributions obtained from fits ZEUS DPDF SJ (continuous line) and ZEUS DPDF C (dashed line), shown for four different values of Q^2 . The shaded error bands show the experimental uncertainty.

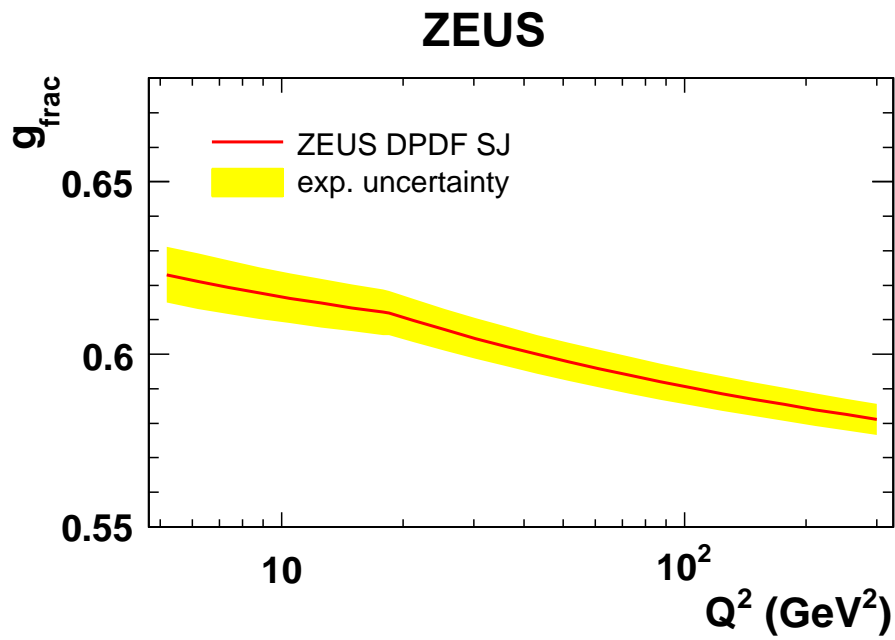


Figure 9: Q^2 dependence of the gluon momentum fraction, g_{frac} , according to the fit ZEUS DPDF SJ. The shaded error band shows the experimental uncertainty.

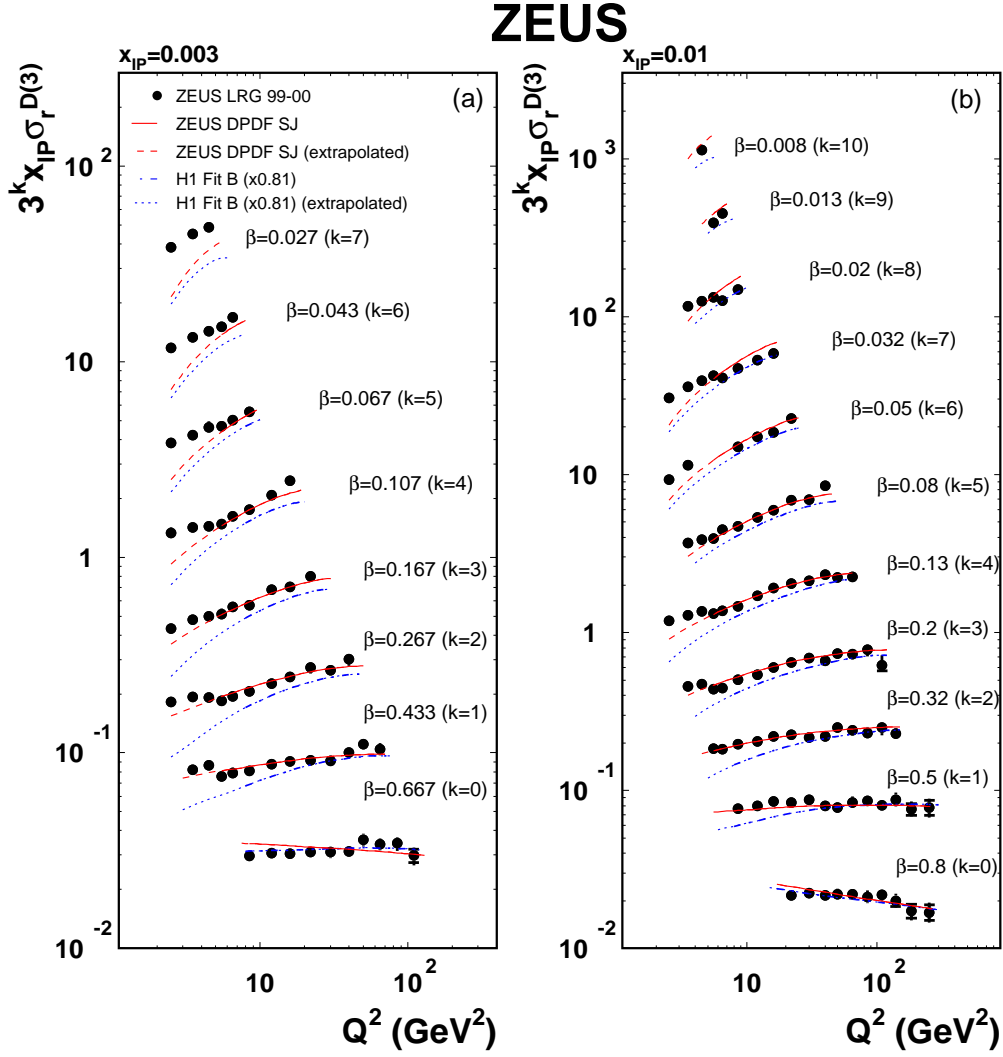


Figure 10: The fit ZEUS DPDF SJ (continuous line) and H1 Fit B [1] (dashed-dotted line) compared to the ZEUS LRG data [9] at (a) $x_{\mathbb{P}} = 0.003$ and (b) $x_{\mathbb{P}} = 0.01$ as a function of Q^2 for different β values. Where visible, the inner error bars show the statistical uncertainties and the full bars indicate the statistical and systematic uncertainties added in quadrature. The H1 predictions are corrected to $M_N = m_p$ via the scaling factor 0.81. The dashed (dotted) lines represent the DGLAP extrapolation beyond the ZEUS (H1) fitted region.

ZEUS

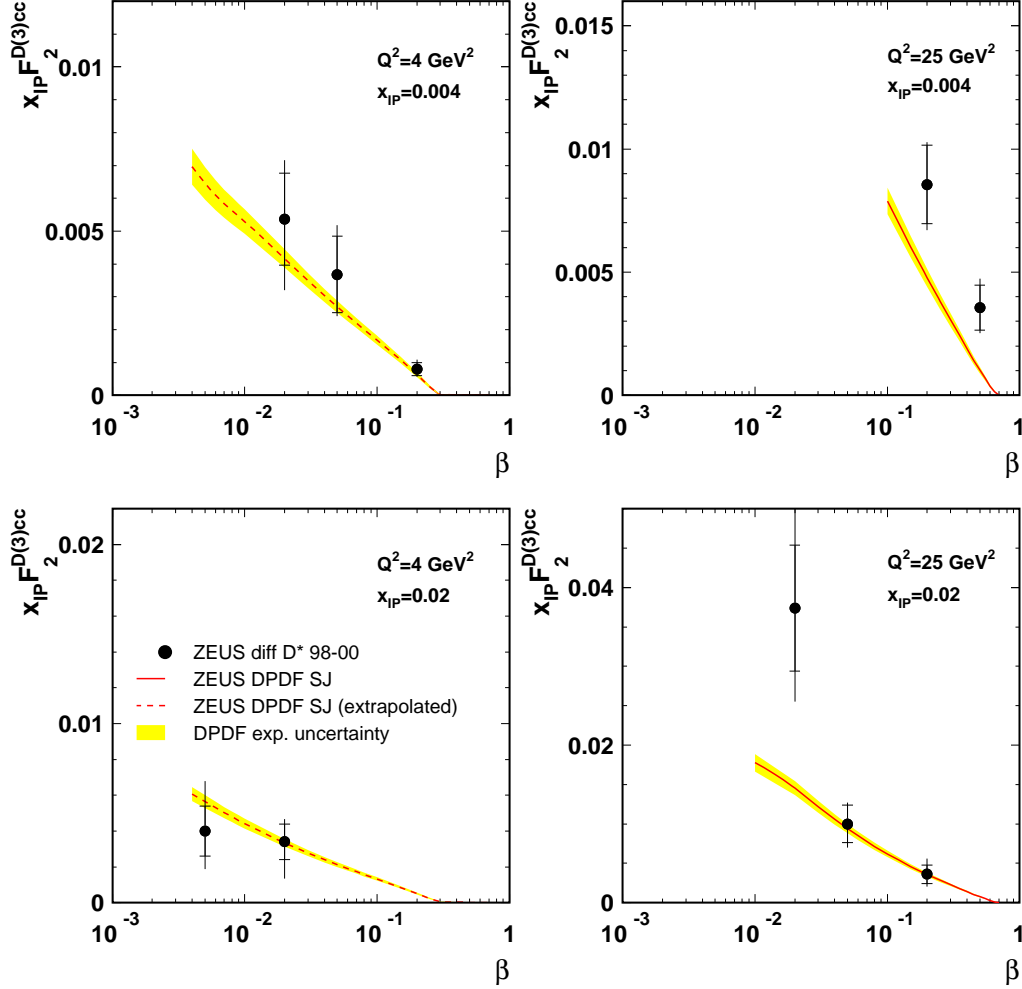


Figure 11: ZEUS DPDF SJ predictions compared to the ZEUS measurement of the charm contribution to the diffractive structure function multiplied by $x_{\mathbb{P}}$, $x_{\mathbb{P}} F_2^{D(3)c\bar{c}}$ [11] as a function of β for different Q^2 and $x_{\mathbb{P}}$ values. The inner error bars show the statistical uncertainties and the full bars indicate the statistical and systematic uncertainties added in quadrature. The dashed lines represent the extrapolation of the predictions beyond the kinematic region where they were obtained. The shaded bands show the DPDF experimental uncertainty.

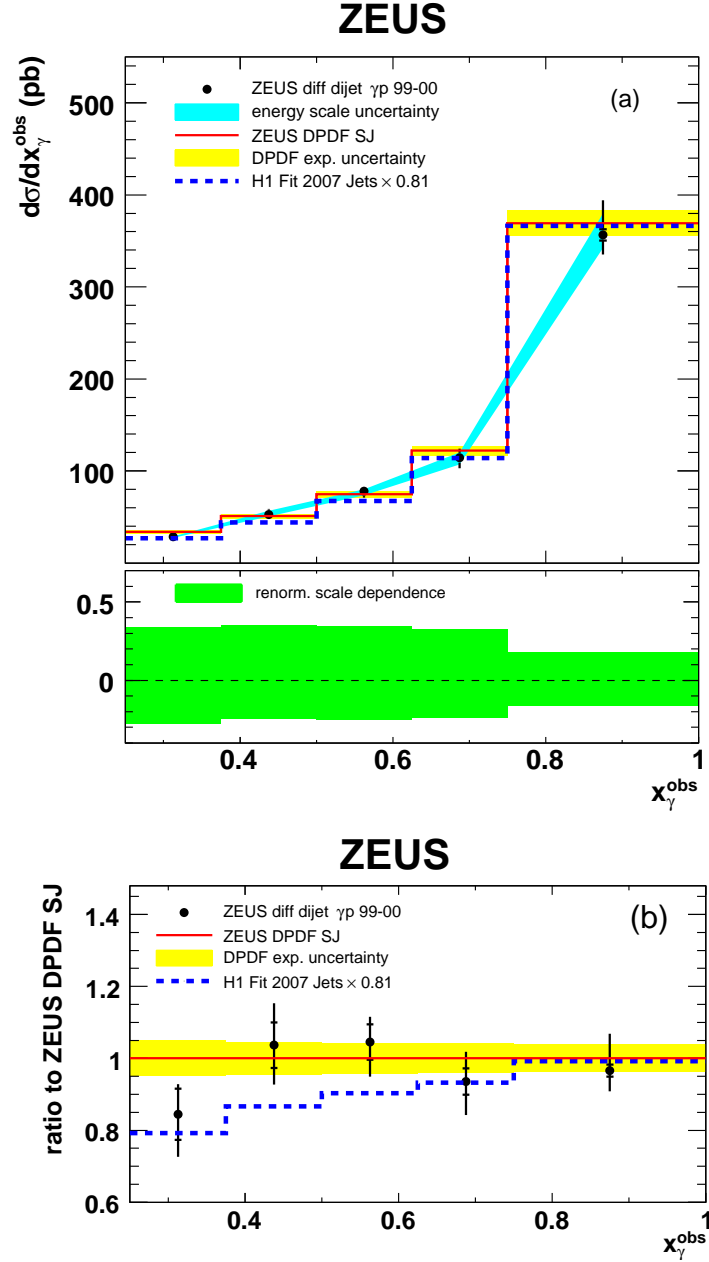


Figure 12: (a) ZEUS DPDF SJ predictions compared to the ZEUS diffractive dijet photoproduction data [12] as a function of x_γ^{obs} . The predictions from H1 Fit 2007 Jets [2] are also shown, corrected to $M_N = m_p$ via the scaling factor 0.81. (b) Ratio of the data and of the H1 predictions to the ZEUS DPDF SJ predictions. The inner error bars show the statistical uncertainties and the full bars indicate the statistical and systematic uncertainties added in quadrature. The dark shaded bands indicate the jet energy scale uncertainty. The light shaded bands show the DPDF experimental uncertainty. The shaded band at the bottom of (a) shows the renormalisation scale uncertainty.

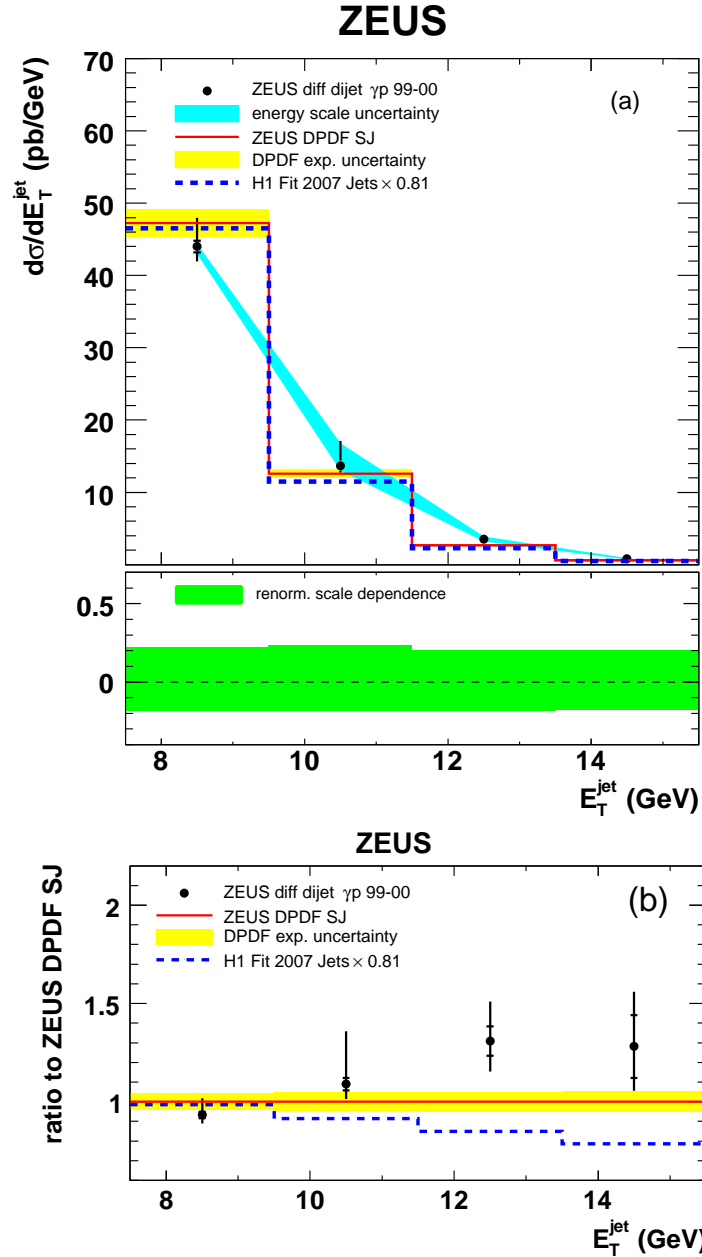


Figure 13: (a) ZEUS DPDF SJ predictions compared to the ZEUS diffractive dijet photoproduction data [12] as a function of E_T^{jet} . The predictions from H1 Fit 2007 Jets [2] are also shown, corrected to $M_N = m_p$ via the scaling factor 0.81. (b) Ratio of the data and of the H1 predictions to ZEUS DPDF SJ predictions. Other details as in caption to Fig. 12.